IEEE Access
Multidisciplinary : Rapid Review : Open Access Journal

Received 11 October 2022, accepted 19 October 2022, date of publication 26 October 2022, date of current version 7 November 2022.

Digital Object Identifier 10.1109/ACCESS.2022.3217527

RESEARCH ARTICLE

Single Event Upsets Under Proton, Thermal, and Fast Neutron Irradiation in Emerging Nonvolatile Memories

GOLNAZ KORKIAN [1], DANIEL LEÓN [2], FRANCISCO J. FRANCO [3], JUAN C. FABERO [1], MANON LETICHE [4], YOLANDA MORILLA [5], PEDRO MARTÍN-HOLGADO [5], (Student Member, IEEE), HELMUT PUCHNER [6], (Senior Member, IEEE), HORTENSIA MECHA [1], AND JUAN A. CLEMENTE [1]

[1]Computer Architecture Department, Facultad de Informática, Universidad Complutense de Madrid (UCM), 28040 Madrid, Spain
[2]Higher Polytechnic School, Universidad Francisco de Vitoria, 28223 Vitoria, Spain
[3]Department of Structure of Matter, Thermal Physics, and Electronics, Facultad de Ciencias Físicas, Universidad Complutense de Madrid (UCM), 28040 Madrid, Spain
[4]Institut Laue-Langevin (ILL), 38000 Grenoble, France
[5]Centro Nacional de Aceleradores, Universidad de Sevilla, 41092 Seville, Spain
[6]Infineon Technologies, Memory Solutions, and Aerospace & Defense, San Jose, CA 95134, USA

Corresponding author: Golnaz Korkian (gkorkian@ucm.es)

This work was supported in part by the Spanish MINECO projects under Grant TIN2017-87237-P and Grant PID2020-112916GB-I00, and in part by the European Union's Horizon 2020 Research and Innovation Program under Grant 101008126.

ABSTRACT In New Space, the need for reduced cost, higher performance, and more prompt delivery plans in radiation-harsh environments have motivated spacecraft designers to use Commercial-Off-The-Shelf (COTS) memories and emerging technology devices. This paper investigates the behavior of state-of-the-art memories manufactured in emerging technologies, including Ferroelectric Random-Access Memory (FRAM), Resistive Random-Access Memory (ReRAM), and Magnetic Random-Access Memory (MRAM), against radiation effects in static and dynamic modes. Radiation-ground tests were conducted under 15-MeV and 1-MeV protons, thermal and 14.8-MeV neutrons leading to various categories of radiation effects. Experimental results will show clear evidence of the robustness of bitcells manufactured using these emerging technologies against radiation, but at the same time, some susceptibility in these devices to suffer radiation effects when working in dynamic mode. Experimental results with the CY15B102Q and CY15B104Q FRAMs (Infineon Technologies), the MB85AS4MT, and MB85AS8MT ReRAMs (Fujitsu), and the MR10Q010CSC and MR25H40CDF MRAMs (Everspin) will be presented and discussed.

INDEX TERMS COTS, emerging memories, FRAM, MRAM, neutrons, new space, protons, ReRAM, thermal neutrons.

I. INTRODUCTION

The democratization of space is an ongoing event involving the introduction of new marketing opportunities. It provides a comprehensive combination of space into society in a tolerable style, either environmentally or economically. Today, large businesses and startups use space as a precious resource to modernize research procedures. The entrepreneurial projects in space introduce a new term called "New Space." The New Space ecosystem emphasizes novel research, development models, economics, and management at a reduced cost [1], [2].

New Space and crucial aerospace missions demand fast growth and lowered costs. The need to reduce expenses and increase reliability for space assignments in harsh environments (extreme temperatures or low bias voltages) has pushed engineers to use Commercial-Off-The-Shelf (COTS) systems in the New Space era. COTS devices are used in an

The associate editor coordinating the review of this manuscript and approving it for publication was Hassan Tariq Chattha.

This work is licensed under a Creative Commons Attribution 4.0 License. For more information, see https://creativecommons.org/licenses/by/4.0/

extensive range of embedded system products, autonomous driving, and High-Performance Computing (HPC) applications. More specifically, in the context of space applications, COTS devices are good candidates for tasks such as Earth observation and communications, exploiting on-board processing, etc., which can be easily implemented in cubesats and nanosats.

One of the critical difficulties of using COTS devices in space derives from the data storage requirements. COTS emerging non-volatile memories such as Magnetic Random-Access Memories (MRAMs), Ferroelectric Random-Access Memories (FRAMs or FeRAMs), and Resistive Random-Access Memories (RRAMs or ReRAMs) have been recently proposed as innovative solutions against radiation effects at less expense than traditional rad-hard solutions [8], [24]. However, COTS devices are not developed to assure an accurate operation in such harsh conditions; therefore, they should be evaluated before using them as avionics or in space missions.

Space is aggressive to electronics due to the existence of cosmic rays, which are composed of streams of charged particles (protons, electrons, heavy ions...). Their interaction with electronic devices impact their performance and this might occasionally result into a critical failure of an entire system. In addition, the increasing miniaturization and complexity of such devices pose additional challenges, such as radiation data analysis and prediction of Single Event Effects (SEE) / Total Ionizing Dose (TID) trends for devices in the International Technology Roadmap for Semiconductors (ITRS) / International Roadmap for Devices and Systems (IRDS). SEEs are classified into soft errors (non-destructive), also called "Single Event Upsets" (SEUs), and hard errors (destructive). A single particle can flip several neighboring cells or one cell, thus leading to a "Multiple Cell Upset" (MCU) or a "Single Bit Upset" (SBU), respectively. If these cells are in the same word, the MCU becomes a "Multiple Bit Upset" (MBU). These errors corrupt data, and occasionally, they are impossible to repair with Error Detection And Correction (EDAC) codes. Single Event Functional Interrupts (SEFIs) happen once an upset of state registers interrupts the regular operation of circuits and enters the device into a different operation mode or locks it up. SEFIs are a type of SEEs taking place at the control sections of the circuit. A software reset or a power-cycling is needed for proper functionality when such an event occurs. Finally, Single Event Latch-ups (SELs) are a type of hard failure which are usually destructive to the system. SELs can appear in Complementary Metal-Oxide-Silicon (CMOS) and Bipolar CMOS (BiCMOS) devices such as electrostatic discharge (ESD) or overvoltage protection circuits [3].

To address the current issues, this research presents an experimental study of the robustness of several non-volatile emerging memories (FRAMs, MRAMs, and ReRAMs) under fast and thermal neutrons, and protons in radiation-ground campaigns that were conducted in collaboration with national and international research institutions, namely: the Centro Nacional de Aceleradores (CNA), in Seville (Spain); the Institut Laue Langevin (ILL), in Grenoble (France); and the Physikalisch-Technische Bundesanstalt (PTB), in Braunschweig (Germany). This research is one of the few works that tested three new and promising non-volatile memory technologies in different densities under diverse radiation sources.

To the best of the authors' knowledge, the radiation effects of neutrons and thermal neutrons on commercial FRAMs, MRAMs against thermal neutrons, and new commercial ReRAMs under thermal and 14.8 MeV (monoenergetic) neutrons have not been studied so far. In addition, with respect to the existing related research in the literature, the novelties found in the results are categorized into four main objectives:

1) To evaluate the SEE sensitivity of two kinds of FRAM, MRAM and ReRAM technologies.
2) To fully consider the behavior of memories in static and dynamic modes.
3) To compare the effects of different radiation sources in different densities in each memory.
4) A complete comparison among emerging memories under different particles and modes.

This paper is organized as follows: Section II introduces the features of emerging non-volatile memories and how particle radiation interacts with matter. Section III describes the experimental setup that was used for testing these memories and details about the radiation facilities. Experimental results and discussions on radiation effects of FRAMs, ReRAMs and MRAMs are provided in Sections IV, V and VI, respectively. Finally, concluding remarks are given in Section VII.

II. EMERGING NON-VOLATILE MEMORIES BASICS

A. FERROELECTRIC RANDOM ACCESS MEMORIES (FRAMs OR FeRAMs)

1) FEATURES OF FRAMs

The concept of producing a memory based on ferroelectric materials first emerged in the master thesis of an MIT student in 1952 [4]; however, the first implementation of a metal–ferroelectric–semiconductor transistor (MFST) appeared in 1974. A common misunderstanding is that "Ferro" implies iron; in reality, ferroelectric memories employ no iron. Ferroelectric properties are available only below a specific threshold temperature, named "Curie temperature", and the material becomes paraelectric above it [5]. The ferroelectric property is marked in a category of materials such as Lead Zirconate Titanate, $\mathrm{Pb}(\mathrm{Z}r_X\mathrm{T}i_{1-X})\mathrm{O}$, in short PZT. The PZT material can switch between two steady states by applying an electric field. As depicted in Figure 1, the cation at the top and bottom is referred to as "up" and "down" polarization, respectively, thus making a memory bit [6].

After eliminating the electric field, ferroelectric materials reveal a remanent polarization [7]; accordingly, the FRAM cell is nonvolatile and is able to keep the information in the memory without refresh. A higher electric field and dielectric constant can yield a higher polarization effect. Figure 2 manifests a typical polarization – displacement (P–D) hysteresis

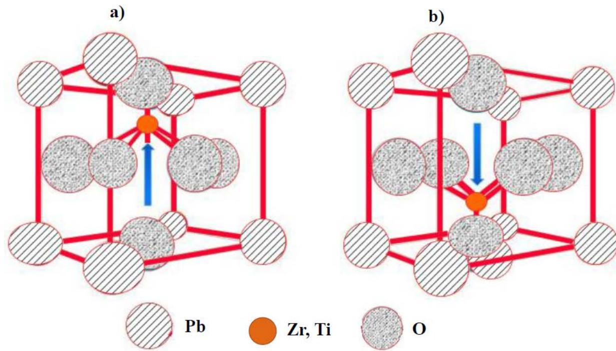

FIGURE 1. Structure of Perovskite ferroelectric crystal and two polarization states a) "on" and b) "off".

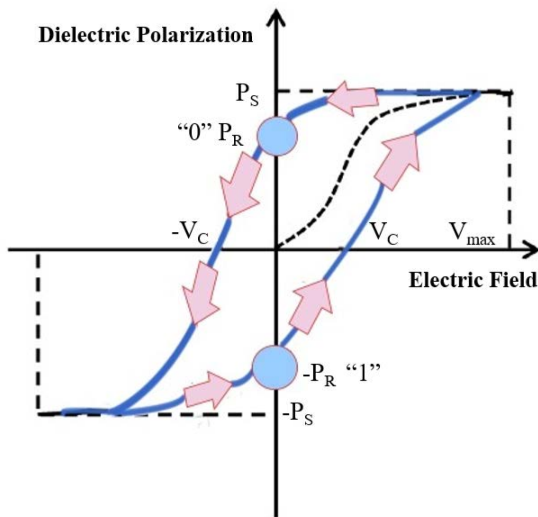

FIGURE 2. Hysteresis curve of ferroelectric materials.

curve as a function of the electric field. Some significant points can be noted from the curve: the permanent polarization points (P_R) exist where the applied electric field is zero. V_C refers to the coercive field, which is the field to move the polarization to zero. P_S means the highest polarization. The two blue circles in the diagram demonstrate stable states with opposite polarization when the electric field is null, representing "0" and "1" bits [6].

Current FRAMs utilize two-transistor, two-capacitor memory (2T2C) cells. Such memory cells provide robust data retention reliability. The one-transistor, one-capacitor (1T1C) technology is an alternative that appeared in the market in 2001. It significantly improves the cost-per-bit ratio and uses a reference voltage in the architecture. Simplified schematics of 1T1C and 2T2C cells are displayed in Figure 3. Ferroelectric memories based on hafnium oxide (HfO_2), Ferroelectric Tunnel Junction (FTJ), as well as ferroelectric field effect transistors (FeFETs) are objects of ongoing research [8], [9].

In summary, the advantages and features that characterize FRAMs are:

- Read access time = write access time < 100 ns.
- Read energy = write energy.

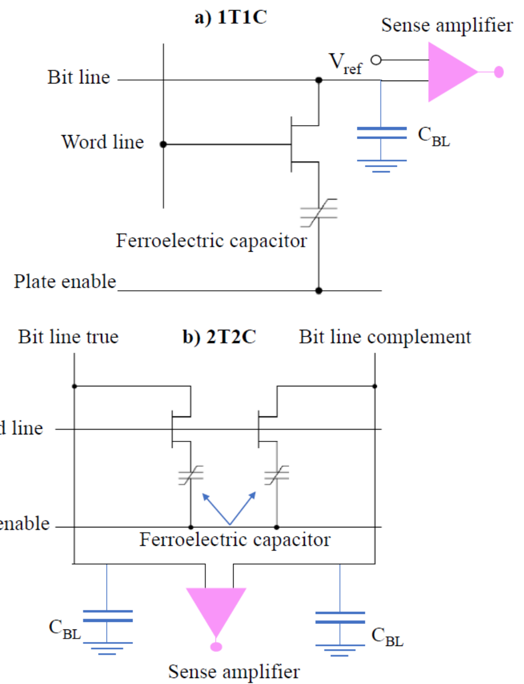

FIGURE 3. Structure of a) 1T1C and b) 2T2C ferroelectric memory cells.

- High write endurance $\sim 10^{14}$ cycles.
- Low power.

Besides, an extensive application base exists for FRAMs, such as in the automotive market, power metering systems, the business printer market, industrial applications, as well as wearable electronics and other energy-efficient applications [10].

2) RADIATION EFFECTS ON FRAMs

Many researchers have investigated the radiation effects on FRAMs quite extensively. Among these, one can classify the contributions discussing the effects of heavy ions, protons, and TID effects.

Devices FM1806 and FM1808, manufactured by Ramtron, were tested against heavy ions in [11]. Wei et al. studied a 90-nm COTS FRAM (the FM28V100) manufactured by Infineon Technologies, using heavy ions and a pulsed laser [12]. Stable upsets, transient upsets, and transient micro-latch-ups in peripheral elements were observed. Stable data upsets concerned several rows, and transient data upsets impacted from hundreds to thousands of rows. Zhang et al. [13] researched SEEs in two COTS FRAMs, the 256-kbit FM18W08 and the 4-Mbit FM22L16, against under heavy ions and a pulsed laser. This study reported at least six SEE classes: SBUs, MBUs, soft SEFIs, hard SEFIs, soft SELs, and hard SELs. The majority of the errors occurred in the peripheral circuitry. The impact of heavy ions has also been analyzed on a 4-Mbit asynchronous FRAM manufactured by Infineon Technologies (FM22L16) in 130-nm CMOS process [14]. Results showed that this memory is susceptible to transient effects in

the peripheral circuitry. A team of NASA also investigated the Ramtron FM22L16 under heavy ions between a range of Linear Energy Transfers (LETs) from 2.7 to 54.1 MeV·cm^2/mg at the TAMU Cyclotron [15]. The results indicate that SEUs and SEFIs happened during these tests. Also, the failure modes of a COTS 130-nm FM22L16 FRAM under heavy ions and pulsed focused X-ray beams were executed in [16]. Mixed failure modes were observed in several types involving individual bits, isolated words, groups of pages, 1-bit-wide columns, entire regions of the memory array, and SEFIs.

Other research has focused on evaluating the SEE sensitivity of these memories under protons. Authors of [15] tested five samples under protons with three energies (198, 140, and 89 MeV), where SEUs and SEFIs were detected. Zanat et al. also executed tests on several FM18L08 memories exposed to X-rays and protons [17]. The authors detected stuck bits (or persistent SEUs) without any data failure, at doses up to 9 Mrad(Si). Also, this study shows that the failure deeply depends on the irradiation temperature. Nuns et al. [18] tested the FM20L08 under 200-MeV protons, where some isolated SEUs were observed.

TID effects on FRAMs have also been studied in the literature. Thus, Shen et al. [19] studied the effects of TID on a 1-Mb parallel FRAM against Cobalt-60 γ rays, X-rays, and electrons. Nuns et al. studied the behavior of the FM20L08 FRAM against TID at a Cobalt-60 facility [18]. Ji et al. also researched the impact of TID in a Cobalt-60 source on the SEE sensitivity of 130-nm FRAMs [20]. They reported that the detected errors in dynamic and static modes are grouped into five categories: single bit errors, multiple bit errors, upsets in sequential (or similar) addresses, and long bursts of errors. Gu et al. [21] investigated the TID effect on a 1-MB parallel FRAM prototype fabricated in a 130-nm CMOS process. The function blocks, including the memory array, sense amplifiers, row decoder, column decoder, and I/O ports were tested using an X-ray microbeam. This study revealed that the ferroelectric part is more robust against TID than the peripheral control circuitry.

Finally, in [22], a group of Devices Under Test (DUTs) were irradiated under 1-MeV neutrons with a fluence of 5×10^{13} n/cm^2. After exposure, they operated normally. The findings revealed that none of the direct and alternating currents (DC and AC) parameters were degraded using neutron irradiation.

B. RESISTIVE RANDOM ACCESS MEMORIES (ReRAMs)

1) FEATURES OF ReRAMs

The primary theory of the memristor (a contraction for ''memory resistor'') device was introduced by professor L. Chua in 1971 [22]. Theoretically, this study presented a fourth fundamental passive element as a new two-terminal circuit element called a memristor. It is illustrated by the relationship existing between the charge and the flux-linkage. In 2008, scientists fabricated the first memristor device. Strukov et al. created a TiO_2 layer, which was sandwiched between two platinum (Pt) electrodes [23]. The proposed physical device employed resistance as a variable to express its state; this is why it was called an RRAM or ReRAM. Between 2005 and 2015 was the golden period of ReRAM investigation.

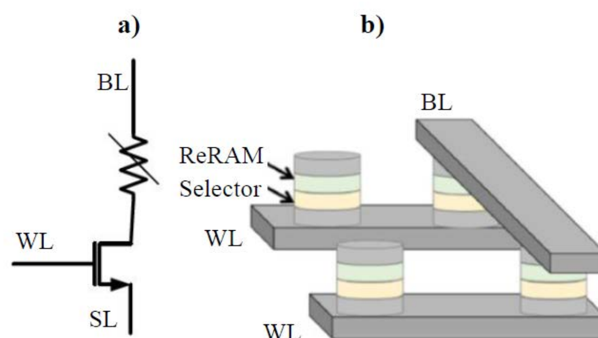

FIGURE 4. a) Schematic of a 1-transistor-1-resistor (1T1R) configuration, b) description of a crosspoint architecture schematic, with the selector and the ReRAM cell [25].

Generally speaking, a ReRAM cell is made of a metal oxide layer, most commonly titanium oxide (TiO_2), tantalum oxide (TaO_x), hafnium oxide (HfO_x) or tungsten oxide (WO_x) that is sandwiched by two metal electrodes [24]. When the ReRAM cell is first manufactured, it is initially in the High Resistance State (HRS). By applying an external voltage pulse across the ReRAM cell allows a transition of the device from HRS (or OFF state) to a Low Resistance State (LRS) (or ON state) to represent the logical ''0'' and ''1'', respectively. The voltage is applied to the Bit Line (BL) in the ''set'' operation and connects the Source Line (SL) to the ground. In the ''reset'' operation, a voltage (VRESET) is applied to the SL and ties the BL to ground [24] as depicted in Figure 4. ReRAMs are non-volatile memories since LRS and HRS keep their values even after removing the external voltage supply.

The advantages of ReRAMs are listed below [26]:

- Small size.
- Low power consumption.
- Non-linear current-voltage (I-V) characteristics.
- Analog behavior is due to the device having many intermediate resistive states.

Lastly, ReRAMs are broadly employed in significant applications, such as crossbar RAM arrays, as well as low-power SRAM designs and sequential circuits [26].

2) RADIATION EFFECTS ON ReRAMs

Some works have studied TID, damage dose effects, and SEEs on devices based on TiO_2, TaO_x and HfO_2. Gonzalez et al. in [25] provided a comprehensive review of radiation upsets on bipolar resistance-switching ReRAMs. This study indicates that these memories are naturally robust against different types of ionizing radiation since they do not directly interact with said radiation.

Bennett et al. [27] examined and modeled SEEs in 1T1R Hf/HfO_2-based ReRAM cells under heavy ions at different bias voltages. The results demonstrated that ReRAM cells are only sensitive in the high resistance state when a voltage higher than 0.65V was employed at the BL. Besides, it was found that individual ions are capable of changing the ReRAMs' resistance to provoke multiple events. Another research was presented by Alayan et al. [28], who irradiated HfO_2-based ReRAMs under heavy ions. Their findings show that these cells are resistant to SEEs. However, the devices would likely be sensitive during a read operation. Further examinations in [29] investigated the Panasonic MN101L, an 8-bit microcontroller with embedded ReRAM against heavy ions and a pulsed laser. SEFIs were observed in the microcontroller due to the structure of the ReRAM consisting in CMOS elements in their peripheral control circuits. Lyu et al. in [30] studied the MB85AS4MT (the same memory studied in this paper), produced by Fujitsu, under heavy ions at a tandem accelerator and a cyclotron in an atmospheric environment. Results revealed that no SEUs nor SELs were observed in the memory under Xe ions (LET was 65 MeV·cm^2/mg). SEFIs happened in the peripheral circuitry of the device when the memory was irradiated with F-ions, Cl-ions, and Ge-ions at LETs of 4.4, 13.1, 3.73 MeV·cm^2/mg, respectively.

Authors in [31] performed tests on a 4-Mbit commercial ReRAM from Fujitsu, MB85AS4MT, to investigate TID effects by a Cobalt-60 source and SEEs provoked by heavy ions and a pulsed laser. Numerous SEFIs in this device were found under heavy ions, and a subsequent pulsed-laser scanning confirmed that events were located in its peripheral circuitry. Maestro-Izquierdo et al. also tested TiN/Ti/HfO_2/W ReRAMs in a cobalt-60 source [32]. Results evidenced that ReRAM cells are hardened against gamma radiation, which is consistent with other previous works.

More considerable research has been accomplished, such as TID studies on a TaO_x-based device under X-rays [33]; as well as gamma rays and 10-keV X-ray irradiation at imec on 55-nm HfO_2/Hf devices [34]. Similarly, more studies have assessed the effects of gamma irradiation on HfO_x-based memory cells [35] and 1-Mrad(Si) exposure on a CMOS-integrated HfO_x-based cell [36]. Generally, findings did not reveal any significant change in switching properties.

C. MAGNETORESISTIVE RANDOM ACCESS MEMORIES (MRAMs)

1) FEATURES OF MRAMs

In Magnetoresistive Random Access Memories (MRAMs), bits are stored through Magnetic Tunnel Junctions (MTJs). An MTJ is comprised of a magnetoresistive layer with a fixed polarization and an additional layer with a variable magnetic polarization (or "free layer"). Both layers are split by a thin dielectric tunnel that operates as a tunnel barrier [37]. The design of an MRAM cell is illustrated in Figure 5.

An external magnetic field can orient the free layer, whereas the reference one remains in a fixed polarization.

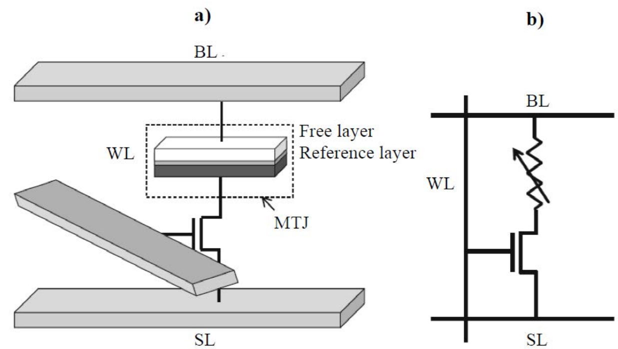

FIGURE 5. Illustration of an MRAM cell: a) structural perspective; b) schematic view (BL: bit line, WL: word line, SL: source line) [25].

If the two layers of the MTJ are polarized in the same direction, the resistance of MTJ is low, indicating logic "0"; in the case that the layers have different directions, the resistance of MTJ is high, showing logic "1". When it comes to writing, for a "reset" operation, the differential voltage between SL and BL is positive; and vice versa for a "set" operation [24]. The read operation is accomplished by measuring the current magnitude via the access transistor at a given gate and drain voltage [38].

The idea of storing data by magnetic polarization in memories dates back to the 1950s [39]. The first commercial MRAMs were invented as an improved version of the structure known as "toggle MRAM" in 2003 [40], [41]. In recent years, considerable research on this technology has been conducted, including on toggle MRAMs, Spin-Torque Transfer (STT) MRAMs, and Thermal-Assisted Switching (TAS) MRAMs.

Generally speaking, STT-MRAMs are nonvolatile memories that feature low voltage, high performance, scalability, remarkable endurance, and reliability compatible with other Back-End-Of-Line (BEOL) CMOS SRAMs [8]. Apalkov et al. [42] presents an extensive review of the developments in MRAM technology over the past 20 years. A helpful work about the physics of STT-MRAMs was provided in [38]. In [43] and [44], authors demonstrated a fully-functional 1-Gb standalone STT-MRAM on 28-nm CMOS and a manufacturable 22-nm FD-SOI 40-Mb embedded MRAM, respectively. Currently, aerospace, robotics, consumer electronics, Internet-of-Things applications, etc., are interested in using STT-MRAM technology.

2) RADIATION EFFECTS ON MRAMs

Various researches have been performed to study the radiation effects on MTJ-based MRAMs. As yet, generally, results have indicated that MRAMs are quite robust against radiation effects [45]. Although the MRAM memory cells are insensitive to radiation, some works such as [6] and [18] have demonstrated that the peripheral circuitry usually included in the chip to carry out I/O operations is susceptible to SELs and TID. In [46], the results show SELs happened at

a LET as low as 7 MeV·cm^2/mg, and a few read errors were observed with TID up to 60 krad(Si) in the MR2A16A device. Heidecker et al. tested MR0A08B manufactured by Everspin to a TID of 75 krad (Si); it was found that the device was resilient against SEUs [47]. Also, results showed no latch-ups at an effective LET of 84 MeV·cm^2/mg.

Authors in [48] studied the SEE susceptibility of an AS008MA12A-C1SC, an 8-Mb STT-MRAM, under heavy ions. SEFIs with large numbers of bitflips happened at a LET of 1.84 MeV·cm^2/mg and higher; however, they disappeared with a power cycle. Other research [49] studied the TID and heavy-ion responses of 55-nm non-volatile STT-MRAMs from Avalanche Technology. Results indicated that these devices were radiation tolerant. A 16-Mb MRAM device, UT8MR2M8, was tested under heavy ions accelerated to 15 MeV / amu [50]. No TID effects ($\leq$1 Mrad(Si)) and SELs ($\leq$100 MeV·cm^2/mg) were observed in this memory. However, SEFIs were observed at a LET of 29.5 MeV·cm^2/mg. Zhao et al. [51] investigated radiation effects of the 180-nm 4-Mbit MRAM (MR2A16AVYS35) under heavy ions. Hard Bit Errors (HBEs) were observed only when the energy was higher than 95.8 MeV.

Katti et al. [45] tested a 256-Mb STT-MRAM under heavy ions, and results proved no failures at energies as high as 84 MeV·cm^2/mg. Kobayashi et al. [52] evaluated the influence of different kinds of heavy ions on a 10-nm CoFeB-MgO MTJ-based MRAM. Their findings demonstrated that recoverable bitflips appear at a threshold LET of about 15 MeV·cm^2/mg. Xiao et al. [53] evaluated the displacement damage on modern pMJT-based STT-MRAMs against 3-MeV Ta ions with fluences ranging from 10^9 to 10^{14} ions/cm^2. No upset was observed at fluences lower than 10^{11} ions/cm^2; however, the structural damage at the CoFeB/MgO interface gradually degrades at higher fluences.

Other works have devoted to study radiation effects of protons on MRAMs. For instance, in [18], the MR2A16A MRAM was tested under 200-MeV protons, resulting in being quite robust. Hughes et al. [54] irradiated STT film stacks and devices using 2-MeV and 220-MeV protons. Results did not reveal any changes in parameters of bit-state, retention, current-in-plane tunneling, or ferromagnetic resonance.

Finally, radiation effects of gamma rays and neutrons on MRAMs have also been studied in the literature. Thus, Ren et al. [55] investigated the gamma-ray and neutron radiation tolerance on MgO-based MTJs. The material was highly tolerant to gamma rays and epithermal neutrons at a fluence of 2.9×10^{15} n/cm^2. Tsiligiannis et al. [56] also made static and dynamic tests on a 4-Mbit 180-nm commercial toggle MRAM using neutrons with energies of 25, 50, and 80 MeV and under a Californium-252 alpha source. Also, researchers in [51] studied radiation effects on a 180-nm 4-Mbit MRAM (MR2A16AVYS35), using gamma rays. The results showed no clear effects. The memory was soft-error resilient in static mode, and more sensitive when dynamic tests were made. Regarding radiation effects provoked by thermal neutrons on COTS MRAMs, to the best of the authors' knowledge, no results were found in the literature. However, pMTJs with sizes relevant for STT-MRAM applications have been found to be resilient to very high fluences of thermal neutron radiation [77].

III. EXPERIMENTAL SETUP

This section illustrates the separate experimental setups that were used for irradiating each memory (FRAMs, MRAMs and ReRAMs). In all the tests, two different methods, namely static and dynamic, were performed on the memories.

Static tests were conducted as follows: First, all 1's, all 0's, or a logical checkerboard ("0 × 55" or "0xAA") pattern was written to the memory; then, it was irradiated while holding it idle, and finally, errors were checked after turning off the beam.

On the other hand, dynamic tests were performed as described below [57]:

- Dynamic Stress (March DS):

$$\uparrow(r1,w0,r0,r0,r0,r0,r0); \uparrow(r0,w1,r1,r1,r1,r1,r1); \uparrow(r1,w0,r0,r0,r0,r0,r0); \downarrow(r0,w1,r1,r1,r1,r1,r1); \downarrow(r1,w0,r0,r0,r0,r0,r0); \uparrow(r0,w1,r1,r1,r1,r1,r1)$$

- March C:

$$\uparrow(w0);\uparrow(r0,w1); \uparrow(r1,w0); \downarrow(r0,w1); \downarrow(r1,w0); \uparrow(r0)$$

March algorithms are constituted by several elements. Each element (shown in the "(...)" bracket pair) and its operations are applied to the entire memory space, and then the algorithm advances to the next cycle. Operations can be read (indicated as 'rX') or written (indicated as 'wX'). X can be 0 or 1, indicating the information that is read or written. Each element is applied in an ascending (↑) or descending (↓) order on all memory addresses.

A. DESCRIPTION OF EMERGING MEMORIES EVALUATED UNDER RADIATION

The emerging nonvolatile memories under study are listed in Table 1. Figure 6 depicts the setup used for each of them. This section will briefly review their features.

1) FRAMs

Two FRAMs were examined: the 2-Mbit CY15B102Q (256K×8 bits) and the 4-Mbit CY15B104Q (512K×8 bits). Both memories employ an advanced ferroelectric process in 130-nm bulk technology manufactured by Infineon Technologies [10]. Bitcells at the CY15B102Q are implemented with a two-transistor, two-capacitor (2T2C) structure, whereas those of the CY15B104Q implement a one-transistor, one-capacitor (1T1C) structure instead. Both devices are accessed via a high-speed Serial Peripheral Interface (SPI), and they present high reliability, low power consumption, as well as the following features:

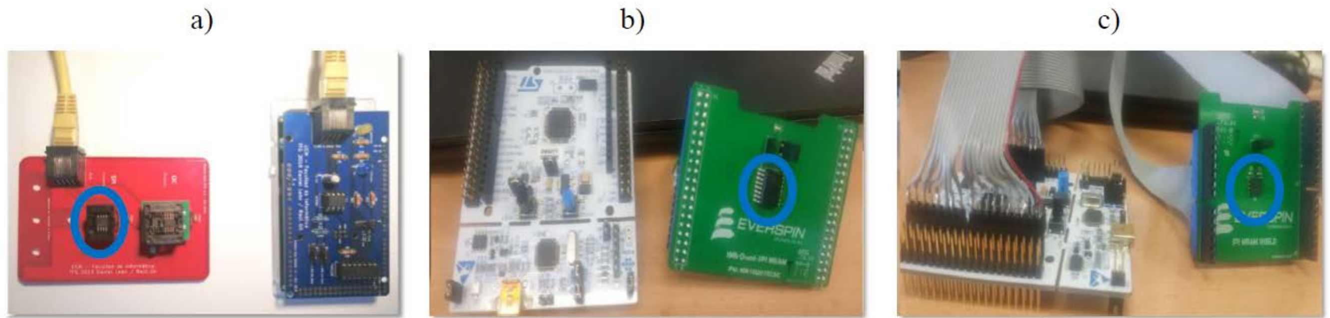

FIGURE 6. Experimental setup for the memories (colored circles indicate the location of memories) for a) FRAMs and ReRAMs, b) the MR10Q010CSC MRAM, and c) the MR25H40CDF MRAM.

- High endurance: 10^{13} reads/writes for the CY15B102Q, and 10^{14} reads/writes for the CY15B104Q.
- 121-year and 151-year data retention for the CY15B102Q and CY15B104Q, respectively.
- Maximum operating frequency up to 25 MHz and 40 MHz for the CY15B102Q and the CY15B104Q, respectively.

The test system was composed by an Arduino DUE (Figure 6a), which executed the test software. A control computer was used for the data retrieval. The Arduino communicated with it by means of a UART. A shield Printed Circuit Board (PCB), connected on top of the Arduino, was designed to correctly route the I/O pins of the memory, as well as to provide variable bias voltage to it. A daughterboard was also developed for hosting the memories, and it was connected to the Arduino by means of a CAT6 twisted pair cable.

2) ReRAMs

The ReRAMs under test were the 4-Mbit MB85AS4MT and 8-Mbit MB85AS8MT, manufactured by Fujitsu, which feature aspect ratios of 512K×8 bits and 1M×8 bits, respectively. The most significant features of these memories are described below:

- High data endurance: 1.2×10^6 times/byte.
- They work by SPI communication protocol.
- Data retention stands for 10 years (+85° C).
- Operating power supply voltage ranges from 1.65 V to 3.6 V.
- The maximum frequency is 5 MHz for the MB85AS4MT and 10 MHz for the MB85AS8MT.

TaO_x-based cells of MB85AS4MT consist in a two-transistor, two-resistor (2T2R) structure, with a common source as depicted in Figure 7. These ReRAMs were tested using the same microcontroller and daughterboard that were used for the FRAMs, which was described above.

3) MRAMs

Two nonvolatile 180 and 130-nm toggle MRAMs (MR10Q010CSC and MR25H40CDF), manufactured by Everspin, were studied.

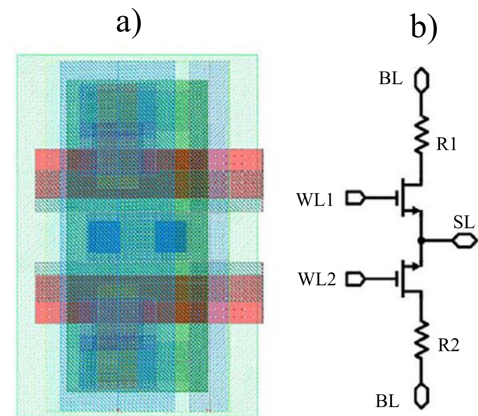

FIGURE 7. a) Layout and b) schematic of the memory cells of the MB85AS4MT that was evaluated under radiation [31].

For testing the MR10Q010CSC, a MR10Q010-EVAL1 evaluation board (also provided by Everspin) was used (see Figure 6b). It has been designed to work with the NUCLEO-L476RG MCU board from ST Microelectronics [58]. The MR10Q010CSC has a capacity of 1-Mb (128K×8 bits) and it is accessed through Quad SPI. Besides, a computer with Internet access and a USB port (with standard A to mini B connectors) is needed to connect the evaluation board to the computer. An online workspace on Mbed website is necessary to upload the code to the memory.

For testing the MR25H40CDF, another evaluation board was also provided by Everspin (this time, the MR25H00-EVAL, see Figure 6c). It is compatible with the Arduino design factor UNO pinout [59]. In this case, the NUCLEO-F411RE MCU board from ST Microelectronics was employed for using it. The rest of the setup description is the same as for the MR10Q010CSC. The most important features of these MRAMs, according to Everspin, are listed below [60], [61]:

- Retention greater than 20 years.
- Automatic data protection on power loss.
- Unlimited write endurance.
- Low-current sleep mode.

TABLE 1. Tested memories.

Manufacturer	Device	Type of memory	Technology process	Density
Infineon	CY15B102Q	FRAM	130-nm	2-Mbit
	CY15B104Q			4-Mbit
Fujitsu	MB85AS4MT	ReRAM	180-nm	4-Mbit
	MB85AS8MT			8-Mbit
Everspin	MR10Q010CSC	MRAM	180-nm	1-Mbit
	MR25H40CDF		130-nm	4-Mbit

B. TEST FACILITIES

This part provides details of the different radiation facilities used to perform tests and measure the SEE sensitivity of the emerging memories that are discussed in this paper. Altogether, 143 experiments were carried out on the memories with high and low-energy protons and thermal and fast neutrons. It should be mentioned that the elements of the setup existing in the irradiation chamber were shielded in all experiments. The irradiations were carried out at a normal incidence angle relative to the direction of the ion beam.

1) CYCLOTRON AT THE CNA

A proton irradiation campaign took place in February 2019 at the Centro Nacional de Aceleradores (CNA), Sevilla (Spain). The experiments were performed using the external beamline installed in the 18/9 IBA compact cyclotron laboratory. The devices were placed at 50-cm from the exit nozzle with a 100-μm aluminum foil as a window; so that the final energy of protons at the surface was 15.3 MeV, whose estimated spread stood on the order of 400 keV. The final energy of the incident beam was obtained using the energy loss data calculated with the SRIM2013 code [62].

The proton flux monitoring was performed by measuring the beam current into an electrically isolated graphite collimator (1 cm of diameter) behind the exit window. A medium flux value was computed in the base of the pulses registered by the counter. Finally, the fluence at the DUT was calculated depending on the exposure time for each run.

Despite the low proton energy, the different device technologies were sensitive enough without delidding them. Furthermore, previous tests conducted by the CNA group with similar devices indicate that the covering (epoxy or similar) thickness on the order of 900-μm as maximum allows working with incident proton energies on the order of 15 MeV to study SEEs in technologies below 130-nm [63], [64].

2) TANDEM LABORATORY AT THE CNA

The irradiation beamline of the 3-MV Tandem Pelletron installed at the CNA [65], was used to perform an irradiation campaign in June 2021. The campaign was performed with protons at an energy of 1.020 MeV $\pm 1\%$, obtained in base to the last calibration of the tandem accelerator. The irradiation was performed at room temperature, and the pressure into the chamber was in the range of 1×10^{-6} mbar. The proton energy at this facility can be configured to a value ranging from 0.6 to 6 MeV. In this case, it was set to 1 MeV.

The DUTs were fitted in a sample holder designed and manufactured to be used in the vacuum chamber of the Tandem CNA laboratory. First, the particle beam is focused on the scintillator placed in the sample holder to obtain a homogeneous spot of a size of 1 cm^2. Afterwards, scanning with a magnetic system increases the full irradiation area. The total fluence is calculated based on the value of the particle density integrated into the complete area. During the focalization process of the beam, only the scintillator was exposed; the samples remain masked behind the slits and one extra aluminum foil, which stops the beam. Complete scanning of 15 cm $\times$ 15 cm was established in this case. The current intensity was measured "in vivo" on the conductive slits and full sample holder, using a Brookhaven 1000c current integrator in the 0.5-nA over 20-nA sensitivity scale.

3) TENIS FACILITY AT THE ILL

Two radiation-ground campaigns were performed at the new Thermal and Epithermal Neutron Irradiation Station (TENIS) hosted by the Institut Laue-Langevin (ILL) in March and September 2021. TENIS replaced D50 as a facility where thermal neutron experiments were executed at the Platform for Advanced Characterisation of Grenoble (PAC-G) [66]. TENIS has a fission-like neutron energy spectrum with a main component of thermal neutrons. Figure 8 directs the Monte-Carlo N-Particle (MCNP) calculated neutron energy spectrum TENIS beamline at the ILL with a high flux reactor.

At the beam exit, a captured flux of 2.86×10^9 n/cm^2/s at nominal reactor power (58 MW) was measured using gold foil activation. The sample position was 49.4-cm away, leading to an estimated captured flux of 2.1×10^9 and 2.4×10^9 n/cm^2/s, in two campaigns, March (reactor power 43 MW) and September 2021 (reactor power 54 MW), respectively.

4) PTB ACCELERATOR FACILITY

The tests were performed under a monoenergetic 14.8-MeV neutron beam at the PTB Ion Accelerator Facility (PIAF), in November 2021.

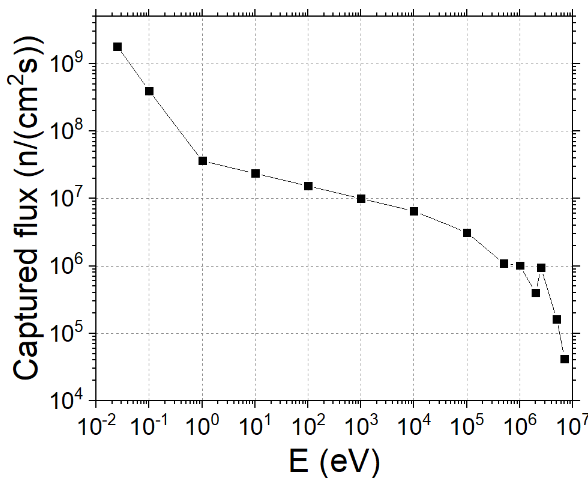

FIGURE 8. Monte Carlo N-Particle (MCNP) calculated neutron energy spectrum on the TENIS beamline at the ILL high flux reactor.

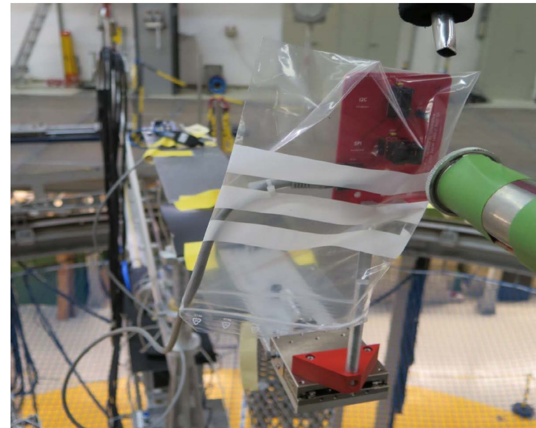

FIGURE 9. Setup for the irradiation of the memory chips at the PTB Ion accelerator facility.

TABLE 2. Informational data on the monoenergetic neutron field used at PIAF.

Reaction	Target	E_n (MeV)	ΔE_n (keV)	Φ_{sc}/Φ_{dir} ($\times 10^{-3}$)
$^3H(d,n)^4He$	Ti(T) 1 mg/cm^2	14.8	435	(2.8 $\pm$ 0.7)%

- Irradiation conditions: The monoenergetic neutron fields were produced according to the general recommendations of the ISO standards [67]. More details on the production and characteristics of the neutron fields are given in Table 2. The mean energy, E_n, and the full width at half maximum (FWHM), ΔE_n, of the direct neutron distribution are nominal values.
  Tests were performed in open geometry in the low-scatter measurement hall (24m $\times$ 30m $\times$ 14m) of the PIAF, at an ambient temperature of (21.5 $\pm$ 1.0)° C. Different PCBs were used to mount the memory chips, which were replaced every time the DUT had to be changed. These were mounted free in the air for each measurement. The distance between the surface of the memory chip and the neutron production target backing was 5.00 $\pm$ 0.1 cm. The Printed Circuit Boards (PCBs), including the memory chips, were covered with a thin plastic bag to avoid contamination, as shown in Figure 9.
- Determination of the neutron fluence: The total neutron fluence Φ is the sum of the fluence Φ_{dir} of the direct neutrons in the target and the fluence Φ_{sc} of neutrons scattered in the target assembly. The value of Φ_{dir} was determined using a De Pangher long counter (details of the measurement and analysis procedures are described in [68]), whereas the value of Φ_{sc} was calculated using the Monte Carlo code TARGET [69]. The ratio Φ_{sc}/Φ_{dir} is listed in Table 2.

IV. FRAMs: EXPERIMENTAL RESULTS AND DISCUSSION

This section discusses the SEE susceptibility of the FRAMs of Table 1 under 15.3-MeV and 1-MeV protons, thermal neutrons, and neutrons of 14.8-MeV. It should be mentioned that in some experiments, SEFIs and destructive SEEs were observed. These errors had in common that 1) either they affected an enormous amount of data addresses and the read contents were random when performing several consecutive readings; or 2) the regular operation of the memory was halted. If a reset in the power supply recovered the contents or operation of the memory, it was considered as a SEFI; otherwise, the error was permanent and counted as a destructive SEE. Also, the setup platform did not have any system to monitor the current consumption of the memories under test, hence the type of destructive SEE (Single Event Burnout or SEB, Single Event Latch-up or SEL, Single Event Gate Rupture or SEGR, as typically classified in the literature [70]) could not be determined. In other occasions, some events initially identified as SBUs or MCUs with little multiplicity (and with non-random erroneous contents) disappeared after performing a power cycle on the memory. These were considered as "unstable" events, following the terminology of Wei et al. [12], who also observed these events on COTS FRAMs under neutrons.

A. EXPERIMENTAL RESULTS ON FRAMs

1) FRAMs - 15.3-MeV PROTONS

12 rounds on the CY15B102Q FRAM were done. The results for each test are detailed in Table 3. Rounds from 5 to 20 minutes were carried out in static mode and one 31-minute round in dynamic mode, at fluxes ranging from 0.24 $\times$ 10^9 to 8.9 $\times$ 10^9 p/cm^2/s.

In the first round, no bitflips were observed, but several events were detected in Rounds 2-4 when tripling the flux with respect to the first round. Isolated SBUs, "unstable" SBUs and "errors-in-row" were observed, as indicated in the table. The latter is a particular kind of multiple events that affected consecutive bits in the same row (physically speaking), following the same terminology as that Ju et al. [71] used in another related work on COTS FRAMs.

TABLE 3. Rounds of irradiation carried out for the FRAMs under 15.3-MeV protons.

N^o	Sample	Test type	Pattern	Fluence ($\times 10^{11}$) (p/cm^2)	Observed events
1	FRAM CY15B102Q (2-Mbit)	Static	0x55	0.85	×
2			0x55	7.5	2 unstable errors-in-row + 1 unstable SBU
3			0xFF	7.3	6 unstable SBUs + 3 SBUs
4			0xAA	7.4	4 unstable errors-in-row + 1 unstable SBU + 2 SBUs
5			0xAA	81	destructive SEE
6			0x00	6.7	×
7			0x00	13	×
8			0x00	93	destructive SEE
9			0x55	24	SEFI
10			0x00	5.9	SEFI
11			0x00	2.9	×
12		Dynamic	March C	4.4	×
13	FRAM CY15B104Q (4-Mbit)	Static	0x55	3.3	×
14		Dynamic	March C	9.2	4 SBUs
15		Static	0x55	6.2	destructive SEE
16			0x55	3.9	×
17			0x55	6.1	×

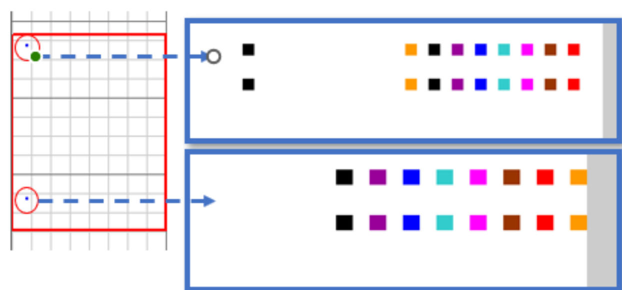

FIGURE 10. 2 errors-in-row and 1 SBU (all unstable), adding 17 bitflips, were observed on the CY15B102Q FRAM under 15.3-MeV protons (Round 2 in Table 3).

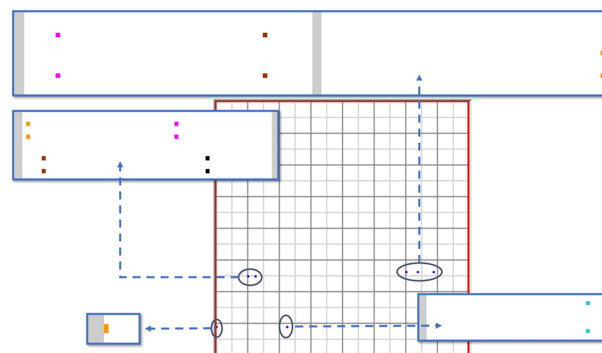

FIGURE 11. 9 isolated SBUs (6 of which were unstable) were observed on the CY15B102Q FRAM under 15.3-MeV protons (Round 3 in Table 3).

Figures 10, 11, and 12 show the bitmap display panel for the bitflips observed in these rounds, obtained with a graphical tool provided by the manufacturer. Each bitflip is showed as 2 colored squares, since the FRAM cells of this memory are 2T-2C and each square indicates a single capacitor being affected by a bitflip. Errors are displayed as square blocks in the location corresponding to the bit's physical die location. The color of a flipped bit is consistent with the I/O line for that bit; it means each bit in a word has a unique color. Non-flipped bits are represented in the white sections, and portions of the die with no active bits (divisions between sections, segments, etc.) are shown as gray.

The highest particle fluences and fluxes belonged to Rounds 5 and 8, which caused permanent damage to the memories (destructive SEE occurred on those occasions), and the tested devices had to be replaced. In Round 9, all addresses were visibly stuck at "0," but no such stuck bits were found after a power cycle; so that was considered as a SEFI. Another SEFI, this time affecting forty thousand addresses with random contents, was also observed in Round 10. Finally, the CY15B102Q received a fluence of 4.4×10^{11} p/cm^2 in a dynamic experiment (Round 12), where no SEEs were observed.

Five more rounds were carried out on the CY15B104Q FRAM (Rounds 13-17 of Table 3). Fluxes ranged from 0.22×10^9 to 0.51×10^9 p/s/cm^2 with exposure times

FIGURE 12. 4 errors-in-raw (unstable) and 3 isolated SBUs, adding 52 bitflips, were observed on the CY15B102Q FRAM under 15.3-MeV protons (Round 4 in Table 3). 2 errors-in-raw affected consecutive addresses, whose starting locations are also indicated in the figure.

TABLE 4. Rounds of irradiation carried out for the FRAMs under 1-MeV protons.

N^o	Sample	Test type	Pattern	Fluence ($\times 10^{10}$) (p/cm^2)	Observed events
1			0x55	4.99	×
2			0x55	16.6	SEFI
3			0x55	0.832	×
4			0x00	0.83	×
5			0xAA	2.5	×
6			0x55	1.3	×
7		Static	0xAA	1.3	×
8	FRAM CY15B102Q (2-Mbit)		0xAA	4	×
9			0xAA	3.3	×
10			0x55	8.3	×
11			0xAA	4	×
12			0xAA	10	SEFI
13		Dynamic	March C	15	destructive SEE
14			March C	13	×
15			March C	25	destructive SEE
16			March C	24	destructive SEE
17	FRAM CY15B104Q (4-Mbit)	Static	0x55	2.2	×
18			0x55	3.4	×
19			0xAA	6.8	×
20			0x55	4.1	×
21			0x55	8.3	×
22			0xAA	4.9	×
23			0xFF	8.6	destructive SEE
24		Dynamic	March C	21	×
25				28.4	destructive SEE

varying from 20 to 30 minutes. Rounds 14 and 15 yielded the most important findings. In Round 14, 4 isolated bitflips were observed, without any evidence of multiple events. The destructive SEE occurred in Round 15 once the device was irradiated with a fluence of 6.2×10^{11} p/cm^2. No SEEs were observed in Rounds 13, 16 and 17.

TABLE 5. Rounds of irradiation carried out for the FRAMs under thermal neutrons.

N^o	Sample	Test type	Pattern	Fluence ($\times 10^{11}$) (n/cm^2)	Observed events
1	FRAM CY15B102Q (2-Mbit)	Static	0x55	6.3	×
2			0xAA	2.52	×
3			0xAA	6.3	×
4			0x55	6.3	×
5			0xFF	14.4	×
6		Dynamic	March C	20	×
7			March DS	28.8	×
8	FRAM CY15B104Q (4-Mbit)	Static	0x55	6.3	×
9			0xAA	6.3	×
10			0xAA	7.2	×
11		Dynamic	March C	40.1	×
12			March DS	31	2 SBUs
13			March DS	58.8	3 SBUs

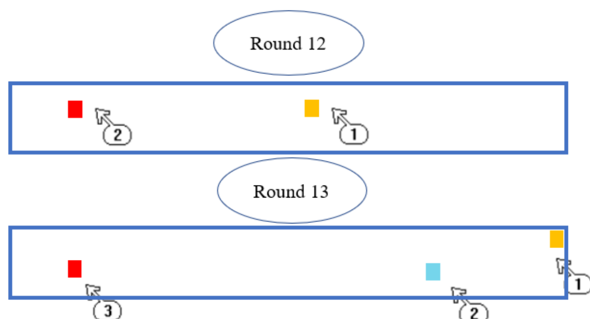

FIGURE 13. SBUs that were observed on the CY15B104Q FRAM under thermal neutrons (Rounds 12 and 13 in Table 5).

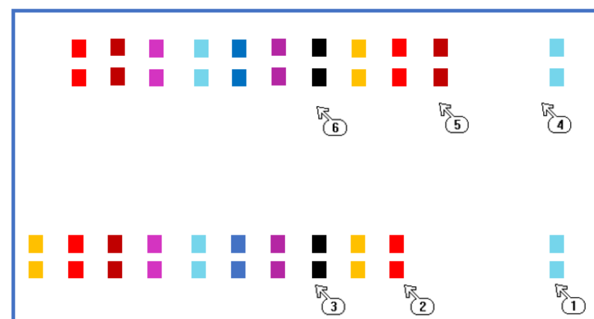

FIGURE 14. 2 errors-in-raw + 2 SBUs, adding 22 bitflips, were observed on the CY15B102Q FRAM under 14.8-MeV neutrons (Round 1 in Table 6).

2) FRAMs - 1-MeV PROTONS

In this case, the FRAMs were delidded prior to the irradiation tests. 25 rounds were performed throughout the campaign, including static and dynamic modes as shown in Table 4.

At first, the CY15B102Q experienced a fluence of 4.99×10^{10} p/cm^2, and no SEE occurred. Thus, the authors decided to increase the fluence to 16.6×10^{10} p/cm^2 in the next round, but this caused damage in the memory, which was attributed to a SEFI. In Rounds 3 to 11, the fluence was lower compared to Round 2, and no errors were observed. In Round 12, the fluence was increased to 10×10^{10} p/cm^2, which again provoked damage on the memory (as in Round 2). Finally, Rounds 13 to 16 were dynamic tests on the CY15B102Q. Among these, only in Round 14 no errors were observed, and in the rest (with fluences ranging from 15×10^{10} to 24×10^{10} p/cm^2), the memory was permanently damaged again.

Rounds 17 to 25 in Table 4 show the tests performed on the CY15B104Q. For the static tests of Rounds 17-23, no errors were observed except for Round 23, where the flux was the highest one among these (8.6×10^{10} p/cm^2), which provoked a permanent damage on the memory. For the dynamic test of Round 24, surprisingly, no errors were observed at a fluence of 21×10^{10} p/cm^2, but a slight increase in the fluence (Round 25) permanently damaged the memory again.

3) FRAMs - THERMAL NEUTRONS

In this case, 13 rounds were performed, which are displayed in Table 5. No errors were observed in static modes, but for the dynamic ones, 2 and 3 SBUs affected consecutive addresses in the the CY15B104Q, in Rounds 12 and 13, respectively. Figure 13 shows the SBUs detected in these rounds.

4) FRAMs - 14.8-MeV NEUTRONS

Finally, 6 more rounds (3 static tests and 3 dynamic ones) were performed on the FRAMs under 14.8-MeV neutrons. Results are presented in Table 6. In Round 1, 2 10-bit errors-in-raw + 2 SBUs were observed, affecting consecutive addresses, as shown in Figure 14. The same tool used for Figures 10-12 was used here again to obtain the XY representation of the observed bitflips.

TABLE 6. Rounds of irradiation carried out for the FRAMs under 14.8-MeV neutrons.

N^o	Sample	Test type	Pattern	Fluence ($\times 10^{10}$) (n/cm^2)	Observed events
1	FRAM CY15B102Q (2-Mbit)	Static	0x55	2.5	2 errors-in-row + 2 SBUs
2			0xAA	2.5	×
3		Dynamic	March C	2.4	1 SBU
4			March DS	2.44	×
5	FRAM CY15B104Q (4-Mbit)	Static	0x55	2.25	×
6		Dynamic	March C	2.21	×

Finally, one more isolated SBU was observed in the same memory when carrying out a dynamic March-C test (Round 3 in Table 6).

B. DISCUSSION ON FRAMs

The tested FRAMs proved to be very resilient against errors provoked by radiation, both under 1-MeV/15.3-MeV protons and thermal/14.8-MeV neutrons. Yet, the following types of errors were found on the FRAMs:

- Unstable SBUs and errors-in-row.
- SBUs.
- SEFIs.
- Destructive SEEs.

Such unstable errors on FRAMs were also reported by Wei et al. [12], this time on the FM28V100 FRAM manufactured by Infineon Technologies, and under 6.1-MeV heavy ions. In that work, the authors believe that these errors might be due to errors in the decoder circuit. These errors were only observed under 15.3-MeV protons and on the 2T-2C CY15B102Q FRAM. Errors-in-row were consistent with the ones observed by Ju et al. [71] on the FM22L16 FRAM (also manufactured by Infineon Technologies), who demonstrated that they originated in N-well resistors in the peripheral circuits, through tests conducted with laser.

SEFIs were observed quite often on the CY15B102Q, for 1-MeV and 15.3-MeV protons. The authors suspect that this is due to errors in the combinatorial logic used to implement I/O operations, which propagate to the rest of the device and provoke communication issues. These SEFIs were similar to the ones detected in other works, such as [11], [13], and [15]. In [15], Scheick et al. examined the FM1806 and FM1808 devices under heavy ions, and found SEFIs due to errors in the devices' peripheral circuitry. In [13], Zhang et al. found, through laser tests in a similar device (the FM18W08 FRAM, manufactured by Infineon) a SEFI-sensitive area exactly in the physical location of the device's peripheral circuit.

Apart from the fact that the CY15B102Q is manufactured with 2T-2C cells and the CY15B104Q, with 1T-1C cells, it was not possible to obtain further information from the manufacturer about the physical implementation of both FRAMs. However, results suggest that the latter is more robust against radiation effects, by the look of Tables 3 and 4, since no SEFIs were observed on the CY15B104Q. The very few SBUs that were spotted (in concordance with other related works on FRAMs under heavy ions [18]) do not allow extracting further conclusions.

TABLE 7. Rounds of irradiation carried out for the MB85AS4MT ReRAM under 1-MeV protons.

N^o	Fluence ($\times 10^{10}$) (p/cm^2)	Observed events
1	0.84	×
2	3.42	×
3	11.4	×
4	13.8	Permanent stuck-at-0
5	3.6	×
6	6.0	×
7	12.0	×
8	18.0	destructive SEE
9	6.00	×
10	12.0	×
11	18.0	Permanent stuck-at-0

Additionally, both memories proved to be sensitive against high proton fluxes. The CY15B102Q suffered permanent damage under 1-MeV 15-25 $\times$ 10^{10} p/cm^2. For 15.3-MeV, higher fluxes (81-93 $\times$ 10^{10} p/cm^2) were needed to provoke the same effect, which is consistent with the well-known fact that low-energy protons contribute more significantly to the total Soft Error Rate (SER) than higher-energy ones [72]. Also, in comparison with the work of Jia et al. [12], who examined the parallel FM28V100 FRAM, it is noteworthy to state that heavy ions never provoked permanent damage on that device. Authors attribute the permanent damage observed on the CY15B102Q and CY15B104Q (see Tables 3 and 4) to some kind of latchup occurred in the combinatorial logic of the devices, which is more complex for serial devices, and traditionally not as radiation-hardened by design as memory cells.

Finally, to the best of the authors' knowledge, radiation effects of neutrons and thermal neutrons have not been

TABLE 8. Rounds of irradiation carried out for the MB85AS4MT ReRAM (4-Mbit) under thermal neutrons.

N^o	Test type	Pattern	Voltage (V)	Fluence ($\times 10^{11}$) (n/cm^2)	Observed events
1	Static	0x55	3.3	6.30	SEFI
2		0x55	3.3	2.52	×
3		0xFF	3.3	6.30	SEFI
4		0xFF	3.3	12.6	SEFI
5		0xFF	3.3	25.2	SEFI
6		0xFF	3.2	12.6	×
7		0xFF	3.09	12.6	×
8		0xFF	2.99	6.30	SEFI
9		0xFF	2.88	6.30	×
10		0xFF	2.78	6.30	Stuck-at-0
11		0x55	2.78	6.30	SEFI
12		0xFF	2.68	6.30	SEFI
13		0xFF	3.3	6.30	×
14		0xFF	3.2	6.30	×
15		0xFF	3.09	6.30	×
16		0xFF	2.99	6.30	SEFI
17		0xFF	2.89	6.30	SEFI
18		0xFF	2.78	6.30	SEFI
19		0xFF	2.68	6.30	SEFI
20		0xFF	2.56	6.30	SEFI
21		0xFF	2.47	6.30	×
22		0xFF	2.37	6.30	SEFI
23		0xFF	2.26	6.30	SEFI
24		0xFF	2.16	6.30	SEFI
25	Dynamic	March C	3.3	37.2	SEFI
26		March C	2.47	16.2	SEFI
27		March C	2.26	49.6	SEFI
28		March DS	3.3	86.4	SEFI

studied on these memories so far. Results shown in Tables 5 and 6 suggest that these devices are quite robust against neutrons, if we compare results with protons. The few amount of such errors do not allow extracting conclusions when comparing the CY15B102Q and the CY15B104Q; or the static and dynamic tests.

V. ReRAMs: EXPERIMENTAL RESULTS AND DISCUSSION

This section discusses the SEE susceptibility of the ReRAMs of Table 1 under low-energy protons, thermal/ 14.8-MeV neutrons.

A. EXPERIMENTAL RESULTS ON ReRAMs

1) ReRAMs - 1-MeV PROTONS

The MB85AS4MT ReRAM was examined against low-energy protons when writing the pattern 0xFF on the whole memory. Results are depicted in Table 7. In Rounds 1-3, no errors were observed, but when increasing the fluence to 13.8×10^{10} p/cm^2, all memory addresses were permanently stuck at 0, so it had to be replaced with a new one. This new device, in Rounds 5-7, did not experience any error, but at a higher fluence (18×10^{10} p/cm^2) again it became unusable (this time, a destructive SEE was observed). The last one that was tested (Rounds 9-11) experienced another permanent stuck-at-0 (Round 11) at high fluence.

2) ReRAMs - THERMAL NEUTRONS

This time, both the MB85AS4MT (4 Mbits of capacity) and MB85AS8MT (8 Mbits of capacity) were exposed to thermal neutrons. Tables 8 and 9 show the rounds of irradiation for both devices. Neutron fluxes were either 2.1×10^9 or 2.4×10^9 n/cm^2/s (because they were carried out at different times in the same facility), but in any case, the table shows the total neutron fluences for each one of the rounds. Also, different

TABLE 9. Rounds of irradiation carried out for the MB85AS8MT ReRAM (8-Mbit) under thermal neutrons.

N^o	Test type	Pattern	Voltage (V)	Fluence ($\times 10^{11}$) (n/cm^2)	Observed events
1	Static	0x55	3.3	6.30	×
2		0xFF	3.3	6.30	×
3		0xFF	3.2	6.47	×
4		0xFF	3.09	6.30	×
5		0xFF	2.99	6.30	×
6		0xFF	2.89	6.30	×
7		0xFF	2.78	6.30	×
8		0xFF	2.68	6.30	×
9		0xFF	2.56	6.30	×
10		0xFF	2.47	6.30	×
11		0xFF	2.37	6.30	×
12	Dynamic	March C	3.3	22.6	SEFI
13		March C	2.37	38.4	SEFI
14		March C	2.99	14.4	SEFI
15		March DS	3.3	18.7	SEFI

TABLE 10. Rounds of irradiation carried out for the ReRAMs under 14.8-MeV neutrons.

N^o	Sample	Test type	Pattern	Fluence ($\times 10^{10}$) (n/cm^2)	Observed events
1	ReRAM MB85AS4MT (4-Mbit)	Static	0x55	0.679	×
2			0xFF	1.36	×
3		Dynamic	March C	1.23	×
4			March DS	2.04	SEFI
5	ReRAM MB85AS8MT (8-Mbit)	Static	0xFF	1.02	×
6		Dynamic	March C	1.25	SEFI

bias voltages were tested in order to evaluate the possible effect of Dynamic Voltage Scaling (DVS) on the memory, which is known to have negative effects on the reliability of SRAMs [63], [64], [73].

As Table 8 indicates, many SEFIs involving communication loss with the memory were observed at the static tests on the MB85AS4MT, which were possible to recover after a power cycle on the memory. A recoverable stuck-at-0 was also observed in Round 10. Tests at bias voltages lower than the nominal one (i.e., <3.3V), seem to point to a higher susceptibility of this memory against radiation effects (especially SEFIs) than biased at 3.3V.

Dynamic tests (Rounds 25-28 in Table 8) were also carried out at different bias voltages. In all of them, SEFIs were observed, consisting in a total malfunction of the dynamic stress test that was carried out (March C or March DS). In all cases, a power cycle solved the problem.

Finally, Table 9 shows the rounds of irradiation made on the MB85AS8MT ReRAM under thermal neutrons. Static and dynamic tests, as well as rounds made at different bias voltages, were carried out. Contrarily to the tests shown in Table 8, the MB85AS8MT showed total immunity against thermal neutrons. However, SEFIs were observed in the 4 dynamic tests made on this memory (Rounds 12-15). The existence of SEFIs in both devices in dynamic tests indicate that the surrounding I/O logic must not be very different in both cases.

3) ReRAMs - 14.8-MeV NEUTRONS

Both ReRAMs were also examined under 14.8-MeV neutrons. The experiments that were carried out are summarized in Table 10. Similarly as with thermal neutrons, no errors were observed in any of these memories in the static tests, but for 2 out of the 3 dynamic ones, SEFIs occurred.

TABLE 11. Rounds of irradiation carried out for the MRAMs under thermal neutrons.

N^o	Sample	Test type	Pattern	Fluence ($\times 10^{11}$) (n/cm^2)	Observed events
1	MRAM MR25H00 (4-Mbit)	Static	0xFF	6.3	×
2			0xAA	6.3	×
3			0x00	12.6	×
4			0x55	6.3	×
5			0x55	7.2	×
6			0x00	7.2	×
7			0xFF	7.2	×
8			0xAA	7.2	×
9		Dynamic	March DS	28.32	×
10	MRAM MR10Q010 (1-Mbit)	Static	0x55	7.2	×
11			0x00	7.2	×
12			0xAA	7.2	×
13			0xFF	7.2	×
14		Dynamic	March C	12.48	SEFI
15			March DS	19.824	SEFI
16			March DS	57.768	×

TABLE 12. Rounds of irradiation carried out for the MRAMs under 14.8-MeV neutrons.

N^o	Sample	Test type	Pattern	Fluence ($\times 10^{10}$) (n/cm^2)	Observed events
1	MRAM MR25H00 (4-Mbit)	Static	0x55	2.75	×
2		Dynamic	March C	1.24	×
3			March C	1.3	×
4	MRAM MR10Q010 (1-Mbit)	Static	0xFF	2.75	×
5		Dynamic	March C	0.99	×
6			March DS	0.99	×

B. DISCUSSION ON ReRAMs

The most common kind of error observed in the tested ReRAMs were SEFIs. In this case, no isolated SBUs were detected, and permanent damage was only provoked for the 1-MeV protons at a very high fluence (>13.8 × 10^{10} p/cm^2).

SEFIs were also observed in other related works on ReRAMs, such as Chen et al. [29], who tested the Panasonic MN101L microcontroller under heavy ions. They attributed such errors to the peripheral circuits, not the memory array. Lyu et al. and Bi et al. also tested the MB85AS4MT ReRAM with a pulsed laser, showing an extremely high robustness of memory cells, but its peripheral IO interface circuit (built with CMOS technology) was susceptible to SEFIs [30], [34]. A team of NASA [74] also used a pulsed laser to test a 180-nm CMOS ReRAM. Again, the resistive memory array was robust against SEUs, but the sense amplifiers were an important source of SEFIs. Finally, Bi et al. [31] observed SEFIs of the MB85AS4MT ReRAM under heavy ions, which was confirmed and exclusively located in the peripheral circuits via pulsed laser scan.

The MB85AS4MT and MB85AS8MT ReRAMs underwent permanent damage considerably less frequently than the FRAMs that were discussed in the previous section. Other related works such as Lyu et al. [30] also showed that the MB85AS4MT was not sensitive against such permanent damage, this time under heavy ions.

A comparison between the MB85AS4MT and the MB85AS8MT (Tables 8 and 9, static tests) clearly indicates that the latter is much more resilient against SEFIs affecting the normal operation of the devices. This is true for thermal neutrons, however for 14.8-MeV ones, the response looks to be quite similar (Table 10).

Finally, both memories were considerably more sensitive against errors when working in dynamic mode, as the FRAMs evaluated in the previous section did. This is consistent with the work of of Bi et al. [31], who also evaluated the MB85AS4MT under TID synergistic effects. To the authors' knowledge, no other works have evaluated the impact of radiation effects in the dynamic operation of ReRAMs.

TABLE 13. An overview of the detected SEEs on FRAMs, ReRAMs, and MRAMs. For simplicity, the table summarizes radiation effects observed in any of the following particle sources: 1-MeV and 15.3-MeV protons, as well as thermal and 14.8-MeV neutrons.

N^o	Sample	Observed events						
		SBUs	SEFIs	Destructive SEEs	Stuck-at-0's	Permanent stuck-at-0's	Unstable SBUs	Unstable errors-in-row
1	FRAM CY15B102Q (2-Mbit)	Yes	Yes	Yes	×	×	Yes	Yes
2	FRAM CY15B104Q (4-Mbit)	Yes	×	Yes	×	×	×	×
3	ReRAM MB85AS4MT (4-Mbit)	×	Yes	Yes	Yes	Yes	×	×
4	ReRAM MB85AS8MT (8-Mbit)	×	Yes	×	×	×	×	×
5	MRAM MR25H00 (4-Mbit)	×	×	×	×	×	×	×
6	MRAM MR10Q010 (1-Mbit)	×	Yes	×	×	×	×	×

VI. MRAMs: EXPERIMENTAL RESULTS AND DISCUSSION

The MRAMs in Table 1 were tested under thermal and 14.8-MeV neutrons. Results are discussed in detail in the following subsections.

A. EXPERIMENTAL RESULTS ON MRAMs

1) MRAMs - THERMAL NEUTRONS

9 and 7 rounds of irradiation were carried out on the MR25H00 and MR10Q010, respectively, under thermal neutrons, as indicated in Table 11.

The MR25H00 did not experience any failure for the 8 static + 1 dynamic tests that were made under neutron fluences up to 12.6×10^{11} n/cm^2 (for static tests) and 28.32×10^{11} n/cm^2 (for the dynamic one). The MR10Q010 was also quite robust in the static tests, but SEFIs were detected in 2 out of the 3 dynamic tests that were carried out.

2) MRAMs - 14.8-MeV NEUTRONS

Finally, 3 tests (1 static + 2 dynamic ones) were done on both MRAMs, as Table 12 indicates. All these rounds yielded no errors. In general, both MRAMs demonstrated to be quite robust against fast neutrons.

B. DISCUSSION ON MRAMs

Other related works on the UT8MR2M8, MR0A08B, MR2A16A, and AS008MA12A-C1SC MRAMs [18], [49], [50], [74] proved them to be as resilient against heavy ions, protons, neutrons and alpha particles as the MR25H00 and MR10Q010 devices discussed in this work. Another work showed that nanoscale pMTJs are robust to high doses of gamma and thermal neutron radiation effects [77].

Following the same trend as with FRAMs and ReRAMs, MRAMs were sensitive against SEFIs in dynamic tests. Tsiligiannis et al. [56] also observed such SEFIs on the 4-Mbit toggle MRAM; and Nuns et al. [18] showed that the MR2A16A device was susceptible to SELs against heavy ions, but no SEUs were seen under 200-MeV protons. As in the case of FRAMs and ReRAMs, a possible explanation could be the CMOS peripheral circuitry being used in reads and writes in the MTJ cells, which is susceptible against radiation [75]. The manufacturer totally confirmed these assumptions about the observed events in the MRAM devices. Finally, other related works [50], [56], [76] also demonstrated that toggle MRAMs, especially in static mode, were immune against SELs, SEUs, or MBUs.

Finally, Table 13 summarizes all the radiation effects observed on the emerging non-volatile memories tested in this paper. As it can be seen in the table, the CY15B102Q FRAM underwent up to 5 types of SEEs, whereas the MR25H00 did not undergo any type of radiation effect.

VII. CONCLUSION

This paper has presented a study of the SEE sensitivity emerging COTS FRAMs, MRAMs, and ReRAMs under 1-MeV and 15.3-MeV protons, thermal and 14.8-MeV neutrons. Static and dynamic tests were carried out in various facilities, showing different vulnerabilities of said devices.

FRAMs were tested in all facilities, where "unstable" SEEs, SBUs, "errors-in-row", stuck-at-errors, SEFIs and hard errors were reported. This classification was possible thanks to the support of Infineon Technologies, who provided a tool to place the affected addresses in the XY plane of the memory. SEFIs were very common in ReRAMs, especially under thermal neutrons and/or for dynamic tests. In this case, it was shown that the MB85AS8MT was more robust than the MB85AS4MT when working in static mode. Finally, MRAMs proved to be very resilient against thermal and 14.8-MeV neutrons, except in dynamic tests.

This research (in line with previous studies on similar devices) shows that, although memory cells in these emerging memories are remarkably robust against radiation effects, observed vulnerabilities in peripheral circuits indicate a potential critical weakness that should be considered, especially in spatial applications.

ACKNOWLEDGMENT

The authors acknowledge the CNA and ILL for the allocated beamtime (TEST-3157 and 3218), and grateful to our colleagues Dr. Ralf Nolte, Dr. Benjamin Lutz, and their team to perform experiments with the neutron source at the PTB. They like to thank the RADNEXT project for the beamtime granted at PTB, and to Infineon Technologies, Fujitsu, and Everspin, for their support.

REFERENCES

[1] Alen. *How to Do Business in Space?* Accessed: Aug. 26, 2020. [Online]. Available: https://alen.space/space-business/

[2] D. Paikowsky, "What is new space? The changing ecosystem of global space activity," *New Space*, vol. 5, no. 2, pp. 84–88, Jun. 2017.

[3] *Space Radiation Effects On Electronics—Single Event Effects*. Accessed: May 11, 2021. [Online]. Available: https://spacetalos.com/news/space-radiation-effects-on-electronics-single-event-effects/

[4] D. A. Buck, "Ferroelectrics for digital information storage and switching," M.S. thesis, Digit. Comput. Lab, Massachusetts Inst. Technol., Cambridge, MA, USA, 1952.

[5] N. Setter, D. Damjanovic, L. Eng, and G. Fox, "Ferroelectric thin films: Review of materials, properties, and applications," *J. Appl. Phys.*, vol. 100, no. 5, 2006, Art. no. 051606.

[6] S. Gerardin and A. Paccagnella, "Present and future non-volatile memories for space," *IEEE Trans. Nucl. Sci.*, vol. 57, no. 6, pp. 3016–3039, Dec. 2010.

[7] T. Mikolajick, C. Dehm, W. Hartner, I. Kasko, M. J. Kastner, N. Nagel, M. Moert, and C. Mazure, "FeRAM technology for high density applications," *Microelectron. Rel.*, vol. 41, no. 7, pp. 947–950, 2001.

[8] M. J. Marinella, "Radiation effects in advanced and emerging nonvolatile memories," *IEEE Trans. Nucl. Sci.*, vol. 68, no. 5, pp. 546–572, May 2021.

[9] Y. M. Coic, O. Musseau, and J. L. Leray, "A study of radiation vulnerability of ferroelectric material and devices," *IEEE Trans. Nucl. Sci.*, vol. 41, no. 3, pp. 495–502, Jun. 1994.

[10] Cypress-FRAM. (2015). *F-RAM Technology Brief*. [Online]. Available: http://www.cypress.com/

[11] L. Scheick, S. Guertin, and D. Nguyen, "SEU evaluation of FeRAM memories for space applications," V1, Root, Jet Propuls. Lab. (JPL), NASA, 2002. [Online]. Available: https://hdl.handle.net/2014/37206, doi: 2014/37206.

[12] J.-N. Wei, H.-X. Guo, F.-Q. Zhang, C.-H. He, A.-A. Ju, and Y.-H. Li, "Single event effects in commercial FRAM and mitigation technique using neutron-induced displacement damage," *Microelectron. Rel.*, vol. 92, pp. 149–154, Jan. 2019.

[13] Z. Zhang, Z. Lei, Z. Yang, X. Wang, B. Wang, J. Liu, Y. En, H. Chen, and B. Li, "Single event effects in COTS ferroelectric RAM technologies," in *Proc. IEEE Radiat. Effects Data Workshop (REDW)*, Jul. 2015, pp. 1–5.

[14] V. Gupta, A. Bosser, G. Tsiligiannis, A. Zadeh, A. Javanainen, A. Virtanen, H. Puchner, F. Saigne, F. Wrobel, and L. Dilillo, "Heavy-ion radiation impact on a 4 Mb FRAM under different test conditions," in *Proc. 15th Eur. Conf. Radiat. Effects Compon. Syst. (RADECS)*, Sep. 2015, pp. 1–3.

[15] M. V. O'Bryan, K. A. LaBel, S. P. Buchner, R. L. Ladbury, C. F. Poivey, T. R. Oldham, M. J. Campola, M. A. Carts, M. D. Berg, A. B. Sanders, and S. R. Mackey, "Compendium of recent single event effects results for candidate spacecraft electronics for NASA," in *Proc. IEEE Radiat. Effects Data Workshop*, Jul. 2008, pp. 11–20.

[16] A. L. Bosser, V. Gupta, A. Javanainen, G. Tsiligiannis, S. D. Lalumondiere, D. Brewe, V. Ferlet-Cavrois, H. Puchner, H. Kettunen, T. Gil, F. Wrobel, F. Saigne, A. Virtanen, and L. Dilillo, "Single-event effects in the peripheral circuitry of a commercial ferroelectric random access memory," *IEEE Trans. Nucl. Sci.*, vol. 65, no. 8, pp. 1708–1714, Aug. 2018.

[17] M. Zanata, N. Wrachien, and A. Cester, "Ionizing radiation effect on ferroelectric nonvolatile memories and its dependence on the irradiation temperature," *IEEE Trans. Nucl. Sci.*, vol. 55, no. 6, pp. 3237–3245, Dec. 2008.

[18] T. Nuns, S. Duzellier, J. Bertrand, G. Hubert, V. Pouget, F. Darracq, J. P. David, and S. Soonckindt, "Evaluation of recent technologies of non-volatile RAM," in *Proc. 9th Eur. Conf. Radiat. Effects Compon. Syst.*, Sep. 2007, pp. 1–8.

[19] J. Shen, W. Li, and Y. Zhang, "Assessment of TID effect of FRAM memory cell under electron, X-ray, and Co- 60 γ ray radiation sources," *IEEE Trans. Nucl. Sci.*, vol. 64, no. 3, pp. 969–975, Mar. 2017.

[20] Q. Ji, J. Liu, D. Li, T. Liu, B. Ye, P. Zhao, and Y. Sun, "Effects of total ionizing dose on single event effect sensitivity of FRAMs," *Microelectron. Rel.*, vol. 95, pp. 1–7, Apr. 2019.

[21] K. Gu, J. J. Liou, W. Li, Y. Liu, and P. Li, "Total ionizing dose sensitivity of function blocks in FRAM," *Microelectron. Rel.*, vol. 55, no. 6, pp. 873–878, May 2015.

[22] L. Chua, "Memristor—The missing circuit element," *IEEE Trans. Circuit Theory*, vol. CT-18, no. 5, pp. 507–519, Sep. 1971.

[23] D. B. Strukov, G. S. Snider, D. R. Stewart, and S. R. Williams, "The missing memristor found," *Nature*, vol. 453, no. 7191, pp. 80–83, 2008.

[24] Y. Xie, *Emerging Memory Technologies: Design, Architecture, and Applications*. Springer, 2013.

[25] Y. Gonzalez-Velo, H. J. Barnaby, and M. N. Kozicki, "Review of radiation effects on ReRAM devices and technology," *Semicond. Sci. Technol.*, vol. 32, no. 8, Aug. 2017, Art. no. 083002.

[26] A. M. Abdelwahed, "Addressing the RRAM reliability and radiation soft-errors in the memory systems," M.S. thesis, Dept. Elect. Comput. Eng., Univ. Waterloo, Waterloo, ON, Canada, 2018.

[27] W. G. Bennett, N. C. Hooten, R. D. Schrimpf, R. A. Reed, and M. H. Mendenhall, "Single- and multiple-event induced upsets in HfO_2/Hf 1T1R RRAM," *IEEE Trans. Nucl. Sci.*, vol. 61, no. 4, pp. 1717–1725, Aug. 2014.

[28] M. Alayan, M. Bagatin, S. Gerardin, A. Paccagnella, L. Larcher, E. Vianello, E. Nowak, and B. De Salvo, "Experimental and simulation studies of the effects of heavy-ion irradiation on HfO_2-based RRAM cells," *IEEE Trans. Nucl. Sci.*, vol. 64, no. 8, pp. 2038–2045, Aug. 2017.

[29] D. Chen, H. Kim, A. Phan, E. Wilcox, K. LaBel, S. Buchner, and A. Khachatrian, "Single-event effect performance of a commercial embedded ReRAM," *IEEE Trans. Nucl. Sci.*, vol. 61, no. 6, pp. 3088–3094, Dec. 2014.

[30] H. Lyu, H. Zhang, B. Mei, Q. Yu, R. Mo, Y. Sun, and W. Gao, "Research on single event effect test of a RRAM memory and space flight demonstration," *Microelectron. Rel.*, vol. 126, Nov. 2021, Art. no. 114347.

[31] J. Bi, B. Li, K. Xi, L. Luo, L. L. Ji, H. B. Wang, and M. Liu, "Total ionization dose and single event effects of a commercial stand-alone 4 Mb resistive random access memory (ReRAM)," *Microelectron. Rel.*, vols. 100–101, Sep. 2019, Art. no. 113443.

[32] M. Maestro-Izquierdo, M. B. Gonzalez, P. Martin-Holgado, Y. Morilla, and F. Campabadal, "Gamma radiation effects on HfO_2-based RRAM devices," in *Proc. 13th Spanish Conf. Electron Devices (CDE)*, Jun. 2021, pp. 23–26.

[33] M. J. Marinella, S. M. Dalton, and P. R. Mickel, "Initial assessment of the effects of radiation on the electrical characteristics of TaO_x memristive memories," *IEEE Trans. Nucl. Sci.*, vol. 59, no. 6, pp. 2987–2994, Dec. 2012.

[34] J. Bi, Z. S. Han, E. X. Zhang, M. W. McCurdy, R. A. Reed, R. D. Schrimpf, and D. M. Fleetwood, "The impact of X-ray and Proton irradiation on HfO_2/Hf-based bipolar resistive memories," *IEEE Trans. Nucl. Sci.*, vol. 60, no. 6, pp. 4540–4546, Dec. 2013.

[35] R. Fang, Y. G. Velo, and W. Chen, "Total ionizing dose effect of γ-ray radiation on the switching characteristics and filament stability of HfO_x resistive random access memory," *Appl. Phys. Lett.*, vol. 104, no. 18, 2014, Art. no. 183507.

[36] S. L. Weeden-Wright, W. G. Bennett, N. C. Hooten, E. X. Zhang, and M. W. McCurdy, "TID and displacement damage resilience of 1T1R HfO_2/Hf resistive memories," *IEEE Trans. Nucl. Sci.*, vol. 61, no. 6, pp. 2972–2978, Dec. 2014.

[37] M. Marinella, "The future of memory," in *Proc. IEEE Aerosp. Conf.*, Apr. 2013, pp. 1–11.

[38] M. D. Stiles and A. Zangwill, "Anatomy of spin-transfer torque," *Phys. Rev. B, Condens. Matter*, vol. 66, Jun. 2002, Art. no. 014407.

[39] *HXNV0100 1Megabit 64K$\times$16 Non-Volatile MagnetoResistive RAM Datasheet*, Honeywell, Charlotte, NC, USA, 2014.

[40] M. Durlam, D. Addie, and J. Akerman, "A 0.18 μm 4Mb toggling MRAM," in *IEDM Tech. Dig.*, Dec. 2003, pp. 6–34.

[41] B. Engel, J. Akerman, and B. Butcher, "A 4-Mb toggle MRAM based on a novel bit and switching method," *IEEE Trans. Magn.*, vol. 41, no. 1, pp. 132–136, Jan. 2005.

[42] D. Apalkov, B. Dieny, and J. M. Slaughter, "Magnetoresistive random access memory," *Proc. IEEE*, vol. 104, no. 10, pp. 1796–1830, Oct. 2016.

[43] S. Aggarwal, K. Nagel, G. Shimon, J. J. Sun, T. Andre, S. M. Alam, H. Almasi, M. DeHerrera, B. Hughes, S. Ikegawa, J. Janesky, H. K. Lee, H. Lu, and F. B. Mancoff, "Demonstration of a reliable 1 Gb standalone spin-transfer torque MRAM for industrial applications," in *IEDM Tech. Dig.*, Dec. 2019, pp. 1–2.

[44] V. B. Naik, K. Lee, K. Yamane, and R. Chao, "Manufacturable 22 nm FD-SOI embedded MRAM technology for industrial-grade MCU and IoT applications," in *IEDM Tech. Dig.*, Dec. 2019, p. 2.

[45] R. R. Katti, S. M. Guertin, J. Y. Yang-Scharlotta, A. C. Daniel, and R. Some, "Heavy ion bit response and analysis of 256 megabit non-volatile spin-torque-transfer magnetoresistive random access memory (STT-MRAM)," in *Proc. IEEE Nucl. Space Radiat. Effects Conf. (NSREC)*, Jul. 2018, pp. 1–4.

[46] D. N. Nguyen and F. Irom, "Radiation effects on MRAM," in *Proc. 9th Eur. Conf. Radiat. Effects Compon. Syst.*, Sep. 2007, pp. 1–4.

[47] J. Heidecker, G. Allen, and D. Sheldon, "Single event latchup (SEL) and total ionizing dose (TID) of a 1 Mbit magnetoresistive random access memory (MRAM)," in *Proc. IEEE Radiat. Effects Data Workshop*, Jul. 2010, p. 4.

[48] M. V. O'Bryan, K. A. LaBel, E. P. Wilcox, D. Chen, E. J. Wyrwas, M. J. Campola, M. C. Casey, J.-M. Lauenstein, A. D. Topper, C. M. Szabo, J. A. Pellish, M. D. Berg, J. W. Lewellen, and M. A. Holloway, "NASA Goddard space flight Center's compendium of recent single event effects results," in *Proc. IEEE Nucl. Space Radiat. Effects Conf. (NSREC)*, Jul. 2018, pp. 1–8.

[49] J. D. Ingalls, M. J. Gadlage, J. Wang, A. M. Williams, D. I. Bruce, and R. Y. Ranjan, "Total dose and heavy ion radiation response of 55 nm avalanche technology spin transfer torque MRAM," in *Proc. IEEE Radiat. Effects Data Workshop*, Jul. 2019, pp. 1–4.

[50] C. Hafer, M. Von Thun, M. Mundie, D. Bass, and F. Sievert, "SEU, SET, and SEFI test results of a hardened 16Mbit MRAM device," in *Proc. IEEE Radiat. Effects Data Workshop*, Jul. 2012, pp. 1–4.

[51] P. X. Zhao, T. Q. Liu, C. Cai, D. Q. Li, Q. G. Ji, Z. He, P. F. Zhai, Y. M. Sun, S. Gu, and J. Liu, "Heavy ion irradiation induced hard error in MTJ of the MRAM memory array," *Microelectron. Rel.*, vols. 100–101, Sep. 2019, Art. no. 113347.

[52] D. Kobayashi, K. Hirose, T. Makino, S. Onoda, T. Ohshima, and S. Ikeda, "Soft errors in 10-nm-scale magnetic tunnel junctions exposed to high-energy heavy-ion radiation," *Jpn. J. Appl. Phys.*, vol. 56, no. 8, 2017, Art. no. 0802B4.

[53] T. P. Xiao, C. H. Bennett, F. B. Mancoff, J. E. Manuel, D. R. Hughart, R. B. Jacobs-Gedrim, E. S. Bielejec, G. Vizkelethy, J. Sun, S. Aggarwal, R. Arghavani, and M. J. Marinella, "Heavy-ion-induced displacement damage effects in magnetic tunnel junctions with perpendicular anisotropy," *IEEE Trans. Nucl. Sci.*, vol. 68, no. 5, pp. 581–587, May 2021.

[54] H. Hughes, K. Bussmann, P. J. McMarr, S.-F. Cheng, R. Shull, A. P. Chen, and S. Schafer, "Radiation studies of spin-transfer torque materials and devices," *IEEE Trans. Nucl. Sci.*, vol. 59, no. 6, pp. 3027–3033, Dec. 2012.

[55] F. Ren, A. Jander, P. Dhagat, and C. Nordman, "Radiation tolerance of magnetic tunnel junctions with MgO tunnel barriers," *IEEE Trans. Nucl. Sci.*, vol. 59, no. 6, pp. 3034–3038, Dec. 2012.

[56] G. Tsiligiannis, L. Dilillo, A. Bosio, P. Girard, A. Todri, A. Virazel, S. S. McClure, A. D. Touboul, F. Wrobel, and F. Saigné, "Testing a commercial MRAM under neutron and alpha radiation in dynamic mode," *IEEE Trans. Nucl. Sci.*, vol. 60, no. 4, pp. 2617–2622, Aug. 2013.

[57] G. Tsiligiannis, L. Dilillo, V. Gupta, A. Bosio, P. Girard, A. Virazel, H. Puchner, A. Bosser, and A. Javanainen, "Dynamic test methods for COTS SRAMs," *IEEE Trans. Nucl. Sci.*, vol. 61, no. 6, pp. 3095–3102, Dec. 2014.

[58] *Everspin Quad SPI MRAM Evaluation Board User Guide, MR10Q010-EVAL1*. Accessed: Feb. 24, 2016. [Online]. Available: https://www.everspin.com/file/157384/

[59] *Everspin SPI MRAM Evaluation Board User Guide, MR25H00-EVAL*. Accessed: Feb. 24, 2016. [Online]. Available: https://www.everspin.com/file/574/

[60] *1 Mb, High Speed Quad SPI MRAM Datasheet*. Accessed: Jun. 2018. [Online]. Available: https://www.everspin.com/getdatasheet/MR10Q010

[61] *4 Mb, SPI Serial Interface Memory Data Sheet*. Accessed: Aug. 2020. [Online]. Available: https://www.everspin.com/getdatasheet/MR20H40

[62] J. F. Ziegler, M. Ziegler, and J. Biersack, "SRIM—The stopping and range of ions in matter (2010)," *Nucl. Instrum. Methods Phys. Res. B, Beam Interact. Mater. At.*, vol. 268, no. 11, pp. 1818–1823, 2010.

[63] M. Rezaei, P. Martin-Holgado, Y. Morilla, F. J. Franco, J. C. Fabero, H. Mecha, H. Puchner, G. Hubert, and J. A. Clemente, "Evaluation of a COTS 65-nm SRAM under 15 MeV protons and 14 MeV neutrons at low VDD," *IEEE Trans. Nucl. Sci.*, vol. 67, no. 10, pp. 2188–2195, Oct. 2020.

[64] M. Rezaei, G. Hubert, P. Martin-Holgado, Y. Morilla, J. C. Fabero, H. Mecha, F. J. Franco, H. Puchner, and J. A. Clemente, "Impact of dynamic voltage scaling on SEU sensitivity of COTS bulk SRAMs and A-LPSRAMs against proton radiation," *IEEE Trans. Nucl. Sci.*, vol. 69, no. 2, pp. 126–133, Feb. 2022.

[65] Y. Morilla, P. Martin-Holgado, A. Romero, J. A. Labrador, B. Fernandez, J. Praena, A. Lindoso, M. Garcia-Valderas, M. Pena-Fernandez, and L. Entrena, "Progress of CNA to become the Spanish facility for combined irradiation testing in aerospace," in *Proc. 18th Eur. Conf. Radiat. Effects Compon. Syst. (RADECS)*, Sep. 2018, pp. 1–5.

[66] C. Weulersse, S. Houssany, N. Guibbaud, J. Segura-Ruiz, J. Beaucour, and F. Miller, "Contribution of thermal neutrons to soft error rate," *IEEE Trans. Nucl. Sci.*, vol. 65, no. 8, pp. 1851–1857, Aug. 2018.

[67] *Calibration Fundamentals of Radiation Protection Devices Related to the Basic Quantities Characterizing the Radiation Field*, ISO, International Standard 8529-2, 2002.

[68] S. Nolte, "PTB contribution to the key comparison CCRI (III)-K11. Comparison of neutron fluence measurements for neutron energies of 27 keV, 565 keV, 2.5 MeV and 17 MeV," in *PTB-Bericht: Neutronenphysik, Fachverlag NW in der Carl*. Bremen, Germany: Schunemann Verlag GmbH, 2018.

[69] D. Schlegel, *TARGET User's Manual*. Braunschweig, Germany: Physikalisch-Technische Bundesanstalt, 2005.

[70] F. W. Sexton, "Destructive single-event effects in semiconductor devices and ICs," *IEEE Trans. Nucl. Sci.*, vol. 50, no. 3, pp. 603–621, Jun. 2003.

[71] A. Ju, H. Guo, F. Zhang, L. Ding, G. Du, J. Guo, X. Zhong, J. Wei, X. Pan, and H. Zhang, "Failure analysis of commercial ferroelectric random access memory for single event effect," *IEEE Trans. Nucl. Sci.*, vol. 69, no. 4, pp. 890–899, Apr. 2022.

[72] N. A. Dodds, M. J. Martinez, P. E. Dodd, M. R. Shaneyfelt, F. W. Sexton, J. D. Black, D. S. Lee, and S. E. Swanson, "The contribution of low-energy protons to the total on-orbit SEU," *IEEE Trans. Nucl. Sci.*, vol. 62, no. 6, pp. 2440–2451, Dec. 2015.

[73] J. A. Clemente, G. Hubert, J. Fraire, F. J. Franco, F. Villa, and S. Rey, "SEU characterization of three successive generations of COTS SRAMs at ultralow bias voltage to 14.2-MeV neutrons," *IEEE Trans. Nucl. Sci.*, vol. 65, no. 8, pp. 1858–1865, Aug. 2018.

[74] M. V. O'Bryan, D. Chen, M. J. Campola, M. C. Casey, A. D. Topper, K. A. LaBel, J. A. Pellish, J.-M. Lauenstein, R. A. Gigliuto, E. P. Wilcox, R. L. Ladbury, M. D. Berg, and R. R. Davies, "Compendium of recent single event effects for candidate spacecraft electronics for NASA," in *Proc. IEEE Radiat. Effects Data Workshop (REDW)*, Jul. 2013, pp. 1–8.

[75] W. Zhao, E. Deng, J. O. Klein, Y. Cheng, and J.-O. Klein, "A radiation hardened hybrid spintronic/CMOS nonvolatile unit using magnetic tunnel junctions," *J. Phys. D, Appl. Phys.*, vol. 47, no. 40, 2014, Art. no. 405003.

[76] R. Bolinder, "Atmospheric radiation effects study on avionics: An analysis of NFF errors," Linköping Univ., Softw. Syst., Inst. Technol., 2013, p. 132.

[77] E. A. Montoya, J.-R. Chen, R. Ngelale, H. K. Lee, H.-W. Tseng, L. Wan, E. Yang, P. Braganca, O. Boyraz, N. Bagherzadeh, M. Nilsson, and I. N. Krivorotov, "Immunity of nanoscale magnetic tunnel junctions with perpendicular magnetic anisotropy to ionizing radiation," *Sci. Rep.*, vol. 10, no. 1, pp. 1–8, Dec. 2020.

GOLNAZ KORKIAN received the B.S. and master's degrees in computer engineering from the Sadjad University of Technology (SUT) and Islamic Azad University, East Azarbaijan Research Branch (IAUT), in 2005 and 2013, respectively. She is currently pursuing the Ph.D. degree with the Complutense University of Madrid (UCM). She worked for three years as a Researcher at the Ferdowsi University of Mashhad (FUM) in the field of temperature sensor networks on FPGA. Her research interests include studying single-event effects on digital circuits, particularly memories, and FPGAs and their use in space missions.

DANIEL LEÓN received the degree in computer engineering and the M.Sc. degree in the Internet of Things from the Complutense University of Madrid (UCM), Spain, the master's degrees in business management and humanities from the Industrial Organization School in Madrid (EOI) and the Universidad Francisco de Vitoria of Madrid (UFV), respectively. He is currently working on a Ph.D. thesis on the radiation effects on RISC-V processors for space missions with the Complutense University of Madrid. For the last four years, he has been a part of the Francisco de Vitoria University, serving as a Professor and the Deputy Director of the computer engineering degree at the Higher Polytechnic School. From 1991 to 2004, he worked as an Engineer, Consultant, and the Director at Hewlett-Packard, Vodafone, EY, and IBM. From 2004 to 2012, he was a managing partner and a major stakeholder of Optiva Media. Following the sale of the company, he served on the several boards of directors, through private investment, before joining UFV, in 2018. During his career, he has been based in Madrid, Spain; Heidelberg, Germany; Costa Mesa, CA, USA; and Sydney, Australia.

FRANCISCO J. FRANCO was born in Montijo, Spain, in 1975. He received the bachelor's degree in physics (electronics) from the University of Seville, Spain, in 1998, and the Ph.D. degree in physics from the Complutense University of Madrid (UCM), in 2005. From 2007 to 2011, he was an Assistant Professor at the Faculty of Physics of UCM, and was promoted to an Associate Professor that year. He was certified by the Spanish ANECA Agency to be eligible as a Full Professor. He has authored or coauthored more than 30 articles in indexed journals and 60 conference papers. He has participated as a member or director of several research projects. His research interests include electronic reliability and mainly associated with radiation effects. He is also a regular reviewer for journals in the field.

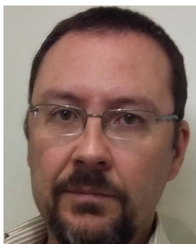

JUAN C. FABERO received the B.S. degree in physics and the Ph.D. degree in computer science from the Complutense University of Madrid (UCM). He is currently an Associate Professor with the Computer Architecture and Automation Department, UCM, in the GHADIR Research Group on Dynamically Reconfigurable Architectures. He is also the Assistant Director of the Computer Architecture and Automation Department, UCM, since 2018. His research interests include design automation, computer architecture, reconfigurable computing, and computer networks.

MANON LETICHE received the Ph.D. degree in material sciences from the University of Lille, France, in 2016. Her work consisted of developing thin film materials for Li-ion micro batteries. Since May 2018, she has been responsible for the characterization and irradiation of electronic components at the Institut Laue-Langevin (ILL) in the framework of the French Institute for Technology Research—IRT Nanoelec.

YOLANDA MORILLA was born in Villamartín, Cádiz, Spain. She received the Fundamental Chemistry degree and the Ph.D. degree from the University of Sevilla, Spain, in 1999 and 2005, respectively. In 2006, she joined as Staff at the Centro Nacional de Aceleradores, a Research Center at the University of Sevilla/CSIC/JA, Spain. First, her research line was related to Ion Beam Analysis. Since 2007, she has been responsible for the different projects in the radiation testing field. Her research interests include radiation effects in electronics and materials, radiation testing, and machine learning-related applications.

PEDRO MARTÍN-HOLGADO (Student Member, IEEE) was born in Sevilla, Spain. He received the physics degree from the University of Seville, Spain, in 2007. He has worked in different companies focused on the space sector. Since 2016, he has been with the National Accelerators Centre, Spain, where he is currently a Predoctoral Researcher. In 2019, he started his status as a Cooperation Associate (COAS) at CERN, where he collaborates with the R2E project. His research interests include dosimetry and radiation effects on electronic devices.

HELMUT PUCHNER (Senior Member, IEEE) received the M.S. and Ph.D. degrees in electrical engineering from Vienna Technical University, in 1992 and 1996, respectively. Since 2002, he has been with Cypress Semiconductor until acquired by Infineon Technologies. Currently, he is responsible for aerospace and defense products at Infineon Memory Solutions.

He has published more than 100 conference/journal articles and holds 39 U.S. patents.

HORTENSIA MECHA was born in 1967. She received the Applied Physics degree from the Complutense University of Madrid (UCM), in 1990, and the Ph.D. degree in physics from UCM, in 1996. Since 2020, she has been a Full Professor of computer architecture and technology at the Computer Architecture and Automation Department, UCM. Her research interests include several aspects of integrated circuits' computer-aided design, with particular emphasis on automated synthesis, reconfigurable computing, and fault tolerance. She has worked with the GHADIR Research Group on Dynamically Reconfigurable Architectures.

JUAN A. CLEMENTE received the degree in computer science and the Ph.D. degree from the Complutense University of Madrid (UCM), Madrid, Spain, in 2007 and 2011, respectively. He is currently an Associate Professor with the Computer Architecture Department, UCM, and a Researcher with the GHADIR Research Group. His research interests include studying single-event effects tolerance of digital circuits, especially commercial-off-the-shelf memories, and their use in harsh environments, such as space. For this research, he collaborates with the TIMA Laboratory, Grenoble-Alpes University, Grenoble, France, and with the ONERA (the French Aerospace Laboratory), Toulouse, France.